On the Excitability of Zero-Group Velocity Lamb Modes Using Normal Mode Expansion Method

PENG ZHANG, PAI WANG, JOHN POPOVICS and XUAN ZHU

ABSTRACT

This study employs the normal mode expansion (NME) method to investigate both symmetric and anti-symmetric zero-group velocity (ZGV) modes. Since a general loading case can always be decomposed into the superposition of the symmetric and anti-symmetric parts corresponding to the symmetric and anti-symmetric modes. The research considers a general loading case and the shear lag model for an adhesive bonding layer to calculate the amplitudes of the generated Lamb modes within and outside of the loading zone. By targeting symmetric (S-) and anti-symmetric (A-) type ZGV modes, the study uses exact analytical solutions and numerical results to validate the effectiveness of the model, ensuring a comprehensive understanding of the behavior of ZGV modes. The influence of the piezoelectric patches' length on the excitability of S- and A-type ZGV modes is also examined. The length of the PZT is a significant factor in determining how effectively the energy can be captured by the targeted modes. Numerical simulations are conducted to observe the behavior of these modes outside the loading zone, providing a broader perspective on their dynamics. Additionally, the study utilizes 2D fast Fourier transform (2D-FFT) results to verify the resonance characteristics of the ZGV modes at the aiming frequency. These results are essential in confirming the theoretical predictions and understanding the practical implications of the ZGV modes. This approach offers valuable insights into the physical behavior of ZGV Lamb modes and their potential applications in various fields.

Peng Zhang, Xuan Zhu, Dept. of Civil & Environmental Engineering, University of Utah, 110 Central Campus Dr., Salt Lake City, UT 84112, U.S.A.
Pai Wang, Dept. of Mechanical Engineering, University of Utah, 1495 E 100 S (1550 MEK), Salt Lake City, UT 84112, U.S.A.
John Popovics, Dept. of Civil and Environmental Engineering, University of Illinois Urbana-Champaign, 205 North Mathews Ave., Urbana, IL 61801, U.S.A.

INTRODUCTION

Piezoelectric wafer active sensors (PWAS) are thin, lightweight devices that can be easily bonded to structural surfaces. They operate on the piezoelectric effect, where mechanical deformation leads to electric charge generation and vice versa. This dual capability allows PWAS to serve as both actuators [1-3] and sensors [3-4], enabling them to excite and detect guided waves such as Lamb waves [5-6] and local resonances [7-8] within waveguide structures. The excitation and reception of these waves are fundamental in measuring the integrity of materials and detecting early defects. Moreover, the capability of PWAS to excite and detect tuned Lamb waves [2, 9] has been explored for structural health monitoring (SHM) purposes. Due to the Lamb wave properties, within the same waveguides, there exist numerous guided wave modes [5, 10], and each wave mode behaves differently. To investigate the behavior of the wave modes and make application of one targeted mode, we need to accurately decompose the modes using the normal mode expansion (NME) method developed by Auld and Kino [11]. As one of the multiple modes, zero-group velocity (ZGV) waves are unique guided wave phenomena characterized by stationary behavior, leading to localized energy confinement [12-17]. This paper examines the excitability of different Lamb wave modes in an aluminum plate under a general loading case and how to maximize the excitability of ZGV waves by tuning the PZT length.

PROBLEM STATEMENT AND METHODS

As shown in Fig. 1, the PWAS was applied on the plate, and the governing equation for elastic waves in elastic solids can be described as

$$\boldsymbol{\nabla}\cdot\boldsymbol{\sigma}+\boldsymbol{f}=\rho\ddot{\boldsymbol{u}} \tag{1}$$

where the $\boldsymbol{\nabla}=\frac{\partial}{\partial x}\hat{\mathbf{x}}+\frac{\partial}{\partial y}\hat{\mathbf{y}}$ indicates the spatial derivative operator with $\hat{\mathbf{x}}$ and $\hat{\mathbf{y}}$ are unit vectors, $\boldsymbol{\sigma}$ is stress tensor, $\boldsymbol{f}$ is body force, ρ is density, $\boldsymbol{u}$ is displacement vector, and $\ddot{}$ indicates second order time differentiation.

Substituting two wave states $(\boldsymbol{u}_1,\boldsymbol{\sigma}_1)$ and $(\boldsymbol{u}_2^*,\boldsymbol{\sigma}_2^*)$ into governing Eq. (1) and making multiplications and subtractions lead to the reciprocity relation,

$$\boldsymbol{\nabla}\cdot(\boldsymbol{\sigma}_1\cdot\boldsymbol{u}_2^*-\boldsymbol{\sigma}_2^*\cdot\boldsymbol{u}_1)=-\boldsymbol{f}_1\cdot\boldsymbol{u}_2^*+\boldsymbol{f}_2^*\cdot\boldsymbol{u}_1 \tag{2}$$

where * indicates complex conjugate.

To decouple the wave modes, we firstly illustrate the orthogonal relation between natural modes. The following two natural states without body forces are considered:

$$\begin{cases}\boldsymbol{\sigma}_1=\boldsymbol{\sigma}_m(y)e^{-\mathrm{i}(k_mx-\omega t)}\\ \boldsymbol{u}_1=\boldsymbol{u}_m(y)e^{-\mathrm{i}(k_mx-\omega t)},\end{cases}\quad\begin{cases}\boldsymbol{\sigma}_2^*=\boldsymbol{\sigma}_N^*(y)e^{-\mathrm{i}(k_N^*x-\omega t)}\\ \boldsymbol{u}_2^*=\boldsymbol{u}_N^*(y)e^{-\mathrm{i}(k_N^*x-\omega t)}.\end{cases} \tag{3}$$

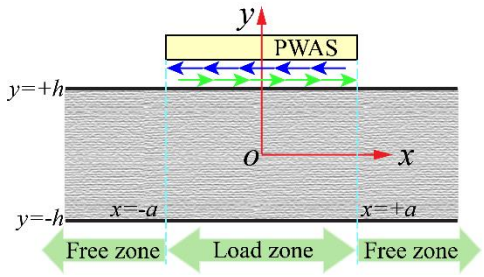

Figure 1. The schematic of the loading under PWAS.

Substituting Eq. (3) into reciprocity relation Eq. (2), taking integral along y-direction, and combining with stress free boundary conditions lead to

$$\mathrm{i}(k_m - k_N^*)\int_{-h}^{h}[\boldsymbol{\sigma}_m(y)\cdot\boldsymbol{u}_N^*(y) - \boldsymbol{\sigma}_N^*(y)\cdot\boldsymbol{u}_m(y)]\cdot\hat{\mathbf{x}}dy = 0 \tag{4}$$

Then, we have the following

$$\mathrm{i}(k_m - k_N^*)P_{mN} = 0 \tag{5}$$

where

$$P_{mN} = -\frac{\mathrm{i}\omega}{4}\int_{-h}^{h}[\boldsymbol{\sigma}_m(y)\cdot\boldsymbol{u}_N^*(y) - \boldsymbol{\sigma}_N^*(y)\cdot\boldsymbol{u}_m(y)]\cdot\hat{\mathbf{x}}dy \tag{6}$$

It is observed that the P_{mN} is non-zero only when $k_m = k_N^*$. For any $k_m \neq k_N^*$, we have $P_{mN} = 0$, which indicates the two modes are orthogonal to each other. Eq. (5) confirms the orthogonal relation between two natural modes, and Eq. (6) is the energy interaction between two modes.

To decouple the modes in a newly excited total wave field, here, we define the total wave field as state-1, and the projection mode field as state-2:

$$\begin{cases}\boldsymbol{\sigma}_1 = \sum a_m(x)\boldsymbol{\sigma}_m(y)e^{\mathrm{i}\omega t}\\ \boldsymbol{u}_1 = \sum a_m(x)\boldsymbol{u}_m(y)e^{\mathrm{i}\omega t},\end{cases}\quad\begin{cases}\boldsymbol{\sigma}_2^* = \boldsymbol{\sigma}_N^*(y)e^{-\mathrm{i}(k_N^*x-\omega t)}\\ \boldsymbol{u}_2^* = \boldsymbol{u}_N^*(y)e^{-\mathrm{i}(k_N^*x-\omega t)}.\end{cases} \tag{7}$$

It is known that the body force vanishes in the natural mode. Follow the similar process and apply the shear lag model for the bounding layer

$$\tau(x) = \tau_0\frac{e^{\Gamma x}-e^{-\Gamma x}}{2}, \tag{8}$$

where τ_0 and Γ are constants due to real loading situations. Then, we obtain

$$a_n(x) = \frac{\mathrm{i}\omega e^{-\mathrm{i}k_N^*x}u_{Nx}^*(h)}{4P_{nN}}(H_n^+ - H_n^-) \tag{9}$$

with

$$H_n^+ = \frac{1}{\mathrm{i}k_N^*+\Gamma}\left[e^{(-\mathrm{i}k_N^*+\Gamma)s} - e^{-(-\mathrm{i}k_N^*+\Gamma)s}\right] \tag{10}$$

$$H_n^- = \frac{1}{\mathrm{i}k_N^*-\Gamma}\left[e^{(-\mathrm{i}k_N^*-\Gamma)s} - e^{-(-\mathrm{i}k_N^*-\Gamma)s}\right] \tag{11}$$

Therefore, the final displacement field is

$$\boldsymbol{u} = \sum a_n(x)\boldsymbol{u}_n(y)e^{-\mathrm{i}\omega t} = \mathrm{i}\omega\sum\frac{\mathrm{i}\omega e^{-\mathrm{i}k_N^*x}u_{Nx}^*(h)}{4P_{nN}}(H_n^+ - H_n^-)\boldsymbol{u}_n(y)e^{-\mathrm{i}\omega t} \tag{12}$$

RESULTS AND DISCUSSION

Based on the analytical solution in Eq. (9), the generated wave modes share the exact same frequency as the input exciting signals in the PZT. The identical frequency of the excited wave modes is due to the forced vibration problem. However, multiple

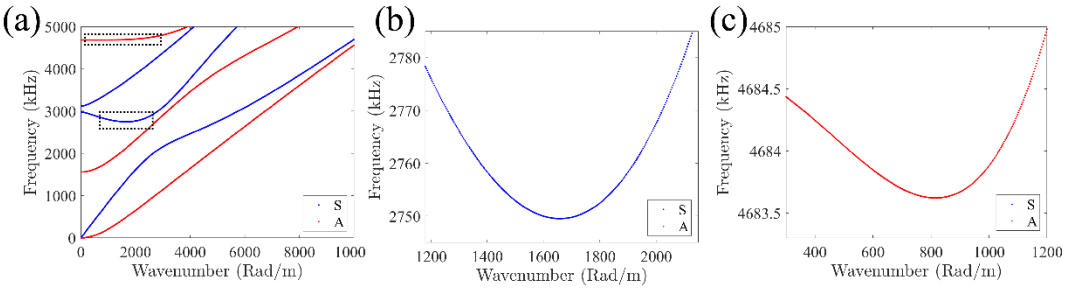

Figure 2. (a) The dispersion of Lamb waves in 1 mm thickness aluminum plate. (b) Symmetric type ZGV. (c) Anti-symmetric type ZGV.

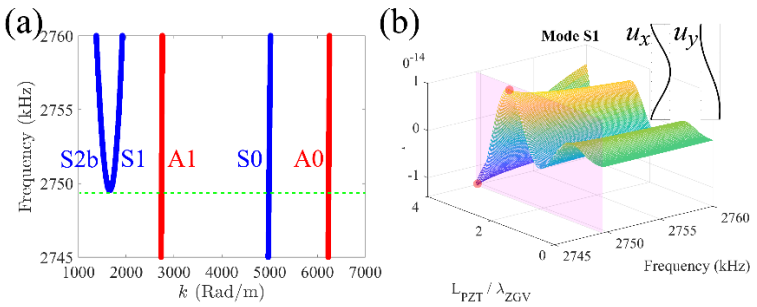

Figure 3. (a) The local dispersion curve of S-type ZGV generation. (b) The amplitudes versus PZT length and frequency of mode S1 and corresponding mode shapes.

modes besides the desired ZGV mode exist under the same exciting frequency and will introduce interference and cause relative errors during measurement. For a 1-mm-thick aluminum plate with Poisson ratio $\upsilon = 0.31$, the dispersion curve is shown in Fig. 2(a). The dashed boxes in Fig. 2(a) are the first S-type and A-type ZGV points, which are illustrated zoomed-in in Fig. 2(b) and Fig. 2(c), respectively. The ZGV mode occurred on the point with horizontal tangent line $c_g = \partial\omega/\partial k = 0$, indicating the velocity of energy flux is zero. For the symmetric loading cases, the excited modes are symmetric with anti-symmetric modes vanishing. As shown in Fig. 3(a), the S-type ZGV point is located at frequency 2749.5 kHz and wavenumber 1658 Rad/m, formed by forward propagating S1 mode and backward propagating S2b mode, with a wavelength of 3.8 mm. For ZGV frequency, shown as vertical planes in Fig. 3(b), the amplitudes grow periodically and exponentially with the increase of PZT length L_{PZT}, precisely as predicted in Eq. (9). However, realistically, the PZT length can only be finite size although the feasible maximum length varies for different materials. For the most commonly used piezoelectric ceramic material, lead zirconate titanate, the size varies from 1 mm to 50 mm in diameter for round shapes or in length for square shapes, with thickness around 0.2 mm to 2 mm. Therefore, to maximize the S-type ZGV mode's amplitude in a 1-mm-thick aluminum plate, we can optimally select the PZTs with lengths 11.48 mm or 15.16 mm, as the two points in Fig. 3(b) by truncating frequency plane crossed amplitudes.

CONCLUSION

In conclusion, we analytically solved the amplitudes of all modes inside the plate under a general loading by using the normal mode expansion method and the shear leg model. We demonstrate that the general loading can always be decoupled into symmetric and anti-symmetric parts. The symmetric loading will only excite the symmetric modes and vice versa. Note that the amplitude excited will increase exponentially with the PZT length with periods depending on the wavenumber. With the limitation of realistic PZT length, we can optimally maximize the amplitude of S- and A-type ZGV modes. This study illuminates the fundamental aspects of the excitability of ZGV modes. It paves a new avenue for the localized energy phenomenon study and maximizing the excitability of desired modes.

REFERENCES

1. Kamal, A. and Giurgiutiu, V., 2014. Shear horizontal wave excitation and reception with shear horizontal piezoelectric wafer active sensor (SH-PWAS). *Smart Materials and Structures*, 23(8), p.085019.
2. Shen, Y. and Giurgiutiu, V., 2015, March. Excitability of guided waves in composites with PWAS transducers. In *AIP Conference Proceedings* (Vol. 1650, No. 1, pp. 658-667). American Institute of Physics.
3. Yu, L., Momeni, S., Godinez, V. and Giurgiutiu, V., 2011, April. Adaptation of PWAS transducers to acoustic emission sensors. In *Nondestructive Characterization for Composite Materials, Aerospace Engineering, Civil Infrastructure, and Homeland Security* 2011 (Vol. 7983, pp. 658-667). SPIE.
4. Huang, H. and Islam, M., 2012, April. PWAS-based wireless acoustic emission sensor. In *Sensors and Smart Structures Technologies for Civil, Mechanical, and Aerospace Systems* 2012 (Vol. 8345, pp. 303-309). SPIE.
5. Su, Z., Ye, L. and Lu, Y., 2006. Guided Lamb waves for identification of damage in composite structures: A review. *Journal of sound and vibration*, 295(3-5), pp.753-780.
6. Gibson, A. and Popovics, J.S., 2005. Lamb wave basis for impact-echo method analysis. *Journal of Engineering mechanics*, 131(4), pp.438-443.
7. Zhang, K., Cui, R., Wu, Y., Zhang, L. and Zhu, X., 2023. Extraction and selective promotion of zero-group velocity and cutoff frequency resonances in bi-dimensional waveguides using the electromechanical impedance method. *Ultrasonics*, *131*, p.106937.
8. Wu, Y., Zhang, K., He, X., Zhang, P., Cui, R., Popovics, J.S. and Zhu, X., Local Resonances in Free and Continuous Welded Rails. *Mechanical Systems and Signal Processing,* Vol 233, 112783, https://doi.org/10.1016/j.ymssp.2025.112783
9. Cès, M., Royer, D. and Prada, C., 2012. Characterization of mechanical properties of a hollow cylinder with zero group velocity Lamb modes. *The Journal of the Acoustical Society of America*, 132(1), pp.180-185.
10. Achenbach, J., 2012. *Wave propagation in elastic solids*. Elsevier.
11. Auld, B.A. and Kino, G.S., 1971. Normal mode theory for acoustic waves and its application to the interdigital transducer. *IEEE Transactions on Electron Devices*, *18*(10), pp.898-908.
12. Tolstoy, I. and Usdin, E., 1957. Wave propagation in elastic plates: low and high mode dispersion. *The Journal of the Acoustical Society of America*, *29*(1), pp.37-42.
13. Prada, C., Clorennec, D. and Royer, D., 2008. Local vibration of an elastic plate and zero-group velocity Lamb modes. *The Journal of the Acoustical Society of America*, *124*(1), pp.203-212.
14. Cès, M., Royer, D. and Prada, C., 2012. Characterization of mechanical properties of a hollow cylinder with zero group velocity Lamb modes. *The Journal of the Acoustical Society of America*, *132*(1), pp.180-185.
15. Zhang, P., Liu, Y., Zhang, K., Wu, Y., Chen, F., Chen, Y., Wang, P. and Zhu, X., 2024. Observation of maxon-like ultrasound in elastic metabeam. *APL Materials*, *12*(3).
16. Wu, Y., Zhang, K., Zhang, P., Zhu, X. and Popovics, J.S., 2023. Dynamic behavior of a zero-group velocity guided mode in rail structures. *JASA Express Letters*, *3*(10).
17. Wu, Y., Cui, R., Zhang, K., Zhu, X. and Popovics, J.S., 2022. On the existence of zero-group velocity modes in free rails: Modeling and experiments. *NDT & E International*, *132*, p.102727.